IRAQI JOURNAL OF APPLIED PHYSICS
Vol. 22, No. 1, January-March 2026, pp. 137-144

Enhancement of Optoelectronic Properties of Electrospun PVA Fibers by Adding Zinc and Cobalt Ions for Photodetection Applications

Duha S. Abd AL–Aziz
Suhad A. Hamdan

Department of Physics,
College of Science,
University of Baghdad,
Baghdad, IRAQ
*Corresponding author:
doha.abd2304@sc.uobaghdad.edu.iq

In this work, polyvinyl alcohol (PVA) nanofibers dual mixed with zinc (Zn) and cobalt (Co) ions were prepared using an electrospinning technique with a precursor solution consisting of, citric acid, and zinc acetate. A polycrystalline structure was revealed for all samples, with peaks corresponding to the semi crystalline-PVA. The branched fibers of mean diameters increased with increasing Co ratio were shown. When the cobalt concentration was increased, the direct bandgap energy decreased from 3.2 to 2.3 eV. A conversion from p- to n-type conductivity was proved with increasing Co ratio. An increase in photoconductivity was observed in the prepared films with increasing Co ratio. The fabricated photodetector demonstrated excellent stability and reproducibility with a notable sensitivity of 503.8% under 380 nm illumination wavelength with a power density of 5.02 mW/cm^2 for the sample prepared at Co:Zn atomic ratio of 4:6.

Keywords: Electrospinning; Nanofibers; Optical properties; Photoconductors
Received: 3 June 2025; Revised: 13 August; Accepted: 20 August 2025; Published: 1 January 2026

1. Introduction

Polyvinyl alcohol (PVA) is a synthetic, water-soluble polymer. It has been widely used in biomedical, environmental, and electronic applications. PVA also offers good optical transparency and thermal stability, making it suitable for functional composite materials. When combined with metal ions, PVA serves as an effective host matrix that facilitates uniform dispersion creating composite nanofibers with enhanced functionality [1]. The metal ions can modify the structural, optical, and electrical properties of the resulting fibers. Upon post-treatment or thermal processing, these metal ions may form metal oxide phases embedded within the PVA nanofiber matrix, making the material highly suitable for optoelectronic applications such as photodetectors and sensors [2].

Zinc oxide (ZnO) is an n-type semiconductor belonging to II-VI group with a band gap of 3.37 eV at room temperature and a binding energy of 60 meV. Its direct band gap and favorable optical properties are responsible for its distinctive optoelectronic behavior [3,4]. Zinc oxide (ZnO) has attracted significant attention for its diverse applications in advanced technologies, including varistors, surface acoustic wave, transparent high-power electronic components, piezoelectric transducers, and UV- emitters [5]. With direct optical band gap varies from 1.45 to 2.7 eV, cobalt oxide (Co_3O_4) is a significant P-type semiconductor and a transition metal oxide. Cobalt oxide is a viable material for use as a pigment for ceramics and glass, as well as in gas sensors and as a catalyst in the hydrocracking of crude fuels [6]. One quick and effective method that makes it easier to produce nanofibers is electrospinning [7]. The electrospinning process is done by applying a high electric field between a conductive collector and a needle containing a viscous polymer solution [8]. By depositing hydrophobic materials, such an approach could produce films with textured surfaces [9]. Nanofibers might therefore be used in optoelectronics, protective textiles, sensors, membrane technologies, and enhanced air filtration based nanofiber production [10]. A flexible method for creating micro- and nanofibers from a variety of solutions (such as hybrid sols, polymer solutions, etc.) is electrospinning [11].

The morphology of ultrafine fibers can be controlled easily by electrospinning [12]. Amazing properties, like a very large surface-to-volume ratio and a high porosity with a small pore size, have been demonstrated through the fibers made using such a technique [13].

A capillary holding a polymer solution or molten polymer precursor receives a high voltage during the electrospinning process. The "Taylor cone" is the point formed when a droplet regarding the polymer solution forms at the capillary's tip. The polymer solution is ejected from the Taylor cone's apex when electrostatic forces surpass the surface tension of the solution

[14,15]. The solvent quickly evaporates when the charged jets of polymer solution approach a collector, and a non-woven fiber mat is gathered on top of the collector. Electrospinning methods were used to create a wide range of polymer nanofibers, including DNA, collagen, polyvinyl alcohol (PVA), and polylactic acid (PLL) [16]. Electrospun nanofibers were used in a variety of fields due to their versatility, such as biomedical sciences, filtration, and optical sensor fields. Inorganic nanoparticle (NP) dispersions in polymer solutions can be instantly transformed into composite nanofibers through the use of electrospinning [17]. With the use of the electrospinning method, Achour et al. have created ZnO as well as Co-doped ZnO composite nanofibers. They employed zinc acetate and PVA as precursors. The nanofibers had an average diameter of about 100 nm after being calcined at 520°C [18]. Lu et al. have successfully create ZnS: Cu/PVA composite nanofibers using of the electrospinning method. A combination of $Cu(Ac)_2$, $Zn(Ac)_2$, and PVA was electrospun after interacting with H_2S to create the fibers [19]. In previous studies, electrospinning has been effectively utilized to produce nanofiber-based photodetectors with enhanced sensitivity [20]. Salim et al. have also synthesized fibers by the electrospinning technique where the spinning solution consisted of polyvinyl alcohol, chitosan, and hyaluronic acid [21]. In a study about electrospun fiber using two different kinds of polymers (PAA and PVA) [22], polymer mixtures have been employed in numerous studies to electrospin materials [23]. While several studies have explored Zn or Co-doped nanofibers individually, there remains a limited understanding of how varying Co:Zn content within PVA electrospun nanofibers affects their optoelectronic behavior.

This study aims to fabricate dual doped (Co, Zn)-PVA composites nanofibers with varying Co:Zn atomic ratios using the electrospinning technique. The motivation behind this work is to investigate how varying the Co content influences the structural, morphological, and optical properties of the composite, as well as its current–voltage (I–V) characteristics.

2. Experimental Part

The nanofibers were synthesized using an electrospinning technique with the use of PVA polymer (Mw= 160,000) (from LOBA CHEMIE PVT, Ltd), zinc acetate dihydrate ($Zn(CH_3COO)_2.\ 2H_2O$) and Cobalt (II) acetate anhydrous ($Co(C_2H_3O_2)_2$).

At first, 0.6 grams of PVA were dissolved in 14 mL of 70% alcohol and stirred for 24 hours. After that, 2.1 g of citric acid was added as a chelating agent. Then 2.195 g of zinc acetate was added gradually, and the solution was stirred for 24 hours before using. Some of the electrospinning solution was placed in a 50 ml syringe of 27 gauge. The distance between the metal needle and the collector was fixed at 13 cm. The flow rate was fixed at 0.6 ml/h. After fixing the glass slides and n-type silicon pieces of (111) orientation on the collector, the voltage was turned on with a voltage of 20 kV. After that the samples were dried with 60 °C for one hour, after that annealing sample with 300°C in air. Repeated procedure for solution with adding cobalt acetate with atomic ratios (Zn:Co= 8:2, 6:4). These ratios were selected based on preliminary trials aimed at optimizing the electrical and optical performance of the nanofibers. The prepared samples were symbolized as listed in table (1).

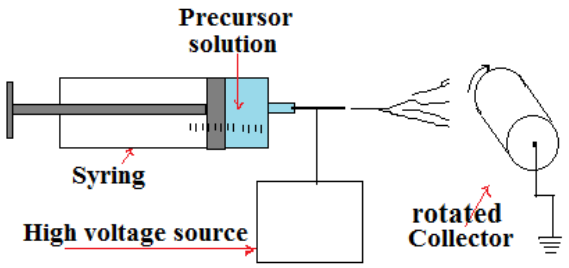

Fig. (1) Schematics of the electrospinning setup

Table (1) Compositions of the prepared samples

Sample	Code
PVA/citric acid/ZnO	D1
PVA/citric acid/ZnO/Co_3O_4 (ZnO:Co_3O_4=8:2)	D2
PVA/citric acid/ ZnO/Co_3O_4 (ZnO:Co_3O_4=6:4)	D3

Cu (Kα) has been utilized as the source of radiation with a wavelength of λ = 1.5405Å in a Shimadzu XRD 6000 diffractometer to analyze the crystal structures regarding the samples. MIRA3 model-TE-SCAN (Dey Petronic Co.) was used to analyze the composition as well as surface morphology of thin films for this study.

The thickness of the fabricated electrospun fiber fabric was estimated using a simple weight-based method, which was found to be approximately 20 µm.

To analyze optical measurements, the Metertech SP-8001 UV-visible spectrophotometer (190-1100 nm) was used. The Hall measurements were carried out using an Ecopia HMS3000 instrument of 0.51 T magnetic fields.

The sensor was fabricated by depositing fiber layer on n-type Si (111) substrates. Prior to deposition, the substrates were ultrasonically cleaned in alcohol followed by an HF dip (1:10 dilution) to remove the native oxide layer and improve film adhesion. To form Ohmic contact, aluminum comb-like electrodes of around 200 nm-thick were deposited on the upper surface of fiber layer by thermal evaporation under high vacuum using an Eduard coating system. Thin wires were connected to the Al electrodes by silver paste to be connected to the examining device.

The electrical behavior of the heterojunction was evaluated through I–V measurements. A Keithley 2450 system was sued to evaluate the prepared samples' current-voltage (I-V) characteristics. Additionally,

using UV light (365 nm, with an average power density of 6.15 mW/Cm^2), photo-response characteristics of UV detectors have been reported.

3. Results and Discussion

Figure (2) shows the XRD patterns of three samples (D1, D2, and D3). The XRD patterns displayed two broad matched the characteristic peaks of semi-crystalline PVA at 12.68° and 20.40°, corresponding to d-values of 6.98 Å and 4.35 Å, respectively. No distinct peaks associated with zinc oxide or cobalt oxide were observed in the patterns of the three samples, due to the low concentration of metal ions in the composite fibers. This indicates that the zinc oxide and cobalt oxide were well-dispersed within the polymer matrix, suppressing their crystallinity. This observation is consistent with previous studies that reported similar XRD patterns dominated by PVA peaks in electrospun composite fibers [24,25].

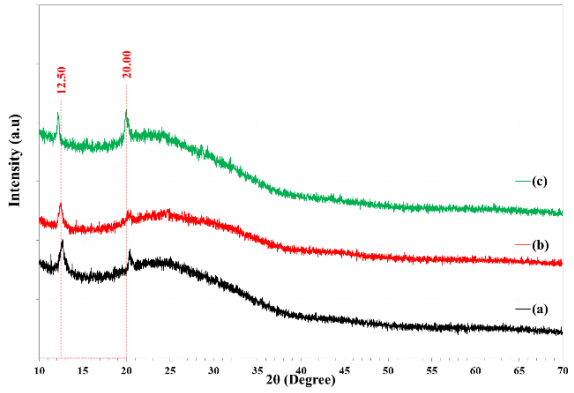

Fig. (2) XRD patterns of (a) D1, (b) D2, and (c) D3

The intensity of diffraction lines was enhanced with increasing the Co content. This indicates that the incorporated cobalt ion may enhance the crystallization. Debye-Scherrer's equation was employed to determine the crystallite size [26]:

$$D = \frac{k\,\lambda}{\beta.cos(\theta)} \qquad (1)$$

where λ represents X-rays wavelength, β represents the full-width at half maximum (FWHM), and θ is the diffraction angle. The crystallite size increased with increasing the cobalt ratio, as shown in table (2), due to the effects of cobalt ions affecting crystal growth differently at different concentrations.

Table (2) XRD parameters of the electrospun samples D1, D2, and D3

Sample	2θ (deg)	d (Å)	FWHM (deg)	Crystallite Size (nm)
D1	12.68	6.98	0.650	12.3
	20.40	4.35	0.437	18.5
D2	12.49	7.08	0.600	13.3
	20.15	4.40	0.355	22.7
D3	12.16	7.28	0.340	23.5
	20.01	4.43	0.382	21.1

The FE-SEM images in Fig. (3) illustrate the surface morphology of electrospun nanofibers prepared for of D1, D2, and D3 samples. Each sample is presented at two magnifications and their corresponding histograms of fiber diameters.

In sample D1, the low-magnification image shows a randomly oriented network of thin nanofibers interspersed with large particle agglomerates, which are likely attributed to undispersed nanoparticles. At higher magnification, the individual fibers appear smooth and uniform in shape, with average diameters of 288 nm. The morphology displays a low fiber density which hinders charge transport. The electrostatic force associated with columbic interactions makes the arrangement randomized and discontinuous [27]. For sample D2, the morphology shows significant improvement. The fibers are more uniform in thickness. The high-magnification image reveals an increase in average fiber diameter to 880 nm. The surface of the fibers remains smooth, and the structure appears highly interconnected. The addition of cobalt precursor at this moderate ratio improves the electrospinning process by optimizing the solution viscosity and conductivity, leading to reduced bead formation and enhanced fiber continuity, improving charge mobility and enhanced light absorption. Sample D3 shows a denser fiber network. The low-magnification image displays a more compact structure with increased fiber intersections, while the high-magnification view reveals fiber diameters reach more than one micrometer. There are visible signs of fiber merging and deformation, which likely result from the excessive conductivity and disrupted jet stability during the electrospinning process. The average fiber diameter becomes 1150 nm. The change in the structural shape with the fiber content agreement with [28].

Figure (4) displays the UV-Vis absorbance and Tauc's plot of the three samples. The absorbance spectra demonstrate strong absorption in the UV and extended to the visible region. However, the absorption gradually decreases as the wavelength increases beyond this range. Although the presence of cobalt ions alongside zinc enhances the material's capability to absorb visible light due to the narrowing band gap. This interaction may contribute to a broadened absorption edge due to defects formation, which could be beneficial for optoelectronic applications.

Because of its improved optical characteristics, including a redshift brought on by a smaller band gap, as reported in the literature, we chose cobalt oxide as the dopant in our research design [29]. The absorption coefficient was calculated from absorbance (A) and the film thickness (t) using the following equation [30]:

$$\alpha = 2.303\, A/t \qquad (2)$$

By analyzing the data and applying Lambert-Beer's law, it turns out that the absorption coefficient in this experiment reflects direct light transmission.

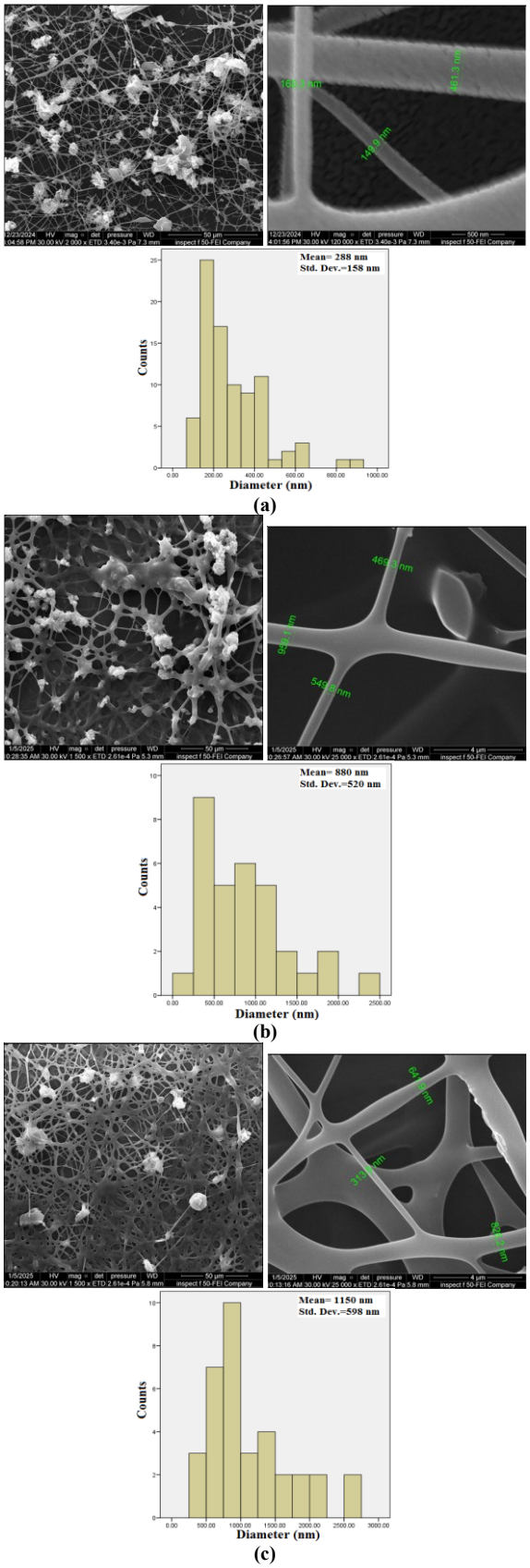

Fig. (3) FE-SEM images at two magnifications and their fiber diameter distribution of (a) D1, (b) D2, and (c) D3

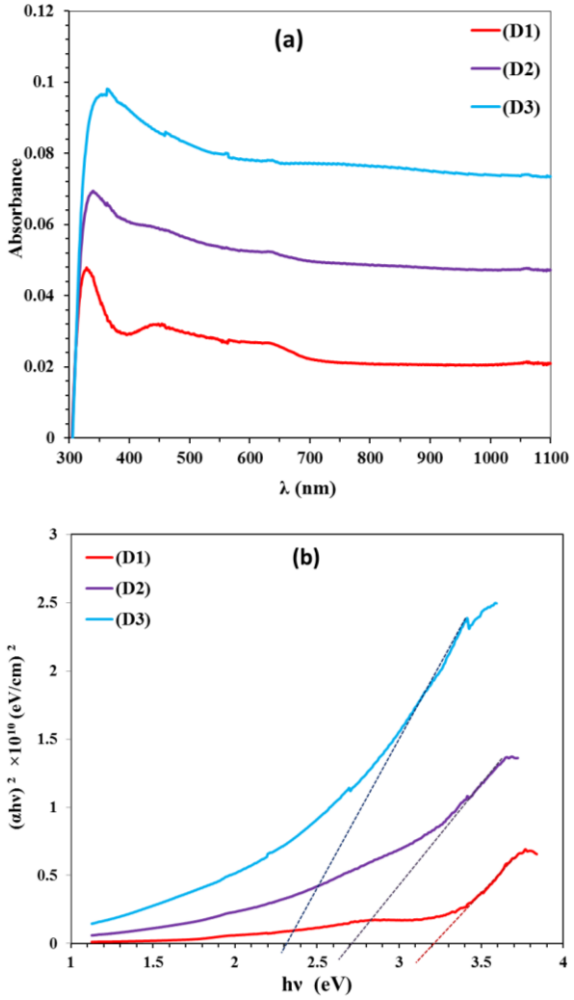

Fig. (4) UV-visible absorption spectra (a) and Tauc plots for the prepared samples (b)

Another investigation supported our findings, indicating that the absorption of UV rays is positively correlated with the concentration of cobalt oxide in ZnO. Using the Tauc relation [31]:

$$\alpha h\upsilon = B(h\upsilon - E_g)^r \quad (3)$$

where r is equal to 0.5, corresponding to every allowed direct optical transition, B represents a constant that relies on electron transitions' probability, h represents Planck's constant, E_g represents the optical energy gap, υ represents photon frequency, α represents the absorption coefficient, and c represents the velocity of light [32].

The energy gap decreased from 3.2 to 2.3 eV with increasing the cobalt content from 0 to 0.4 as shown in Fig. (4) and table (3). The findings indicate that the crystallite size tends to increase with increasing cobalt oxide content, the energy gap decreases. This inverse correlation suggests that the primary factor influencing the optical band gap on the crystallite size and the material's compositional changes.

Table (3) Results of the energy gap compared with the crystallite size

Sample	E_g (eV)	Crystallite Size (nm)
D1	3.2	12.3
D2	2.7	13.3
D3	2.3	23.5

Hall coefficient (R_H), charge carrier's conductivity type, Hall mobility (μ_H), and carriers' concentration (n_H) were estimated from Hall measurements as listed in table (4). Sample D1 (without cobalt oxide) has high resistivity and low conductivity, D2 significant improvement in conductivity decrease in resistivity increase in conductivity significant increase in mobility compared to D1 and sample D3 increase in resistivity and decrease in conductivity compared to D2 and decrease in mobility. An improvement in electrical performance was observed when cobalt oxide was added at a ratio of 20%. While, further increasing to 40 % (sample D3) resulted in converting to n-type, increased resistivity, reduced conductivity, and lower mobility compared to D2. The observed p-type to n-type conversion in sample D3 can be attributed to the substitutional occupation of cobalt ions of Zn^{2+} sites that introduce additional donor-like states. This substitution may also create oxygen vacancies which act as n-type dopants, leading to a transition from p-type to n-type conductivity.

The current–voltage (I–V) characteristics are essential for evaluating the performance of photodetectors. Photoconductivity is governed by carrier generation, trapping, recombination processes, and carrier mobility [33]. Figure (5) presents the I–V curves of the three samples (D1, D2, and D3), measured under dark and illuminated using UV light of 6.15 mW/cm^2 average power density, at a bias voltage range of –5 to +5 V. All samples exhibit asymmetric I–V curves typical of diode-like junction behavior.

At lower bias voltages (0–1.5 V), the dark current remains relatively low, across all samples, due to the charge trapping and recombination process. As the applied voltage increases beyond 1.5 V, the drift velocity of carriers overcomes the influence of trap centers, and the current begins to increase more linearly with voltage, indicating reduced transit time and more efficient charge transport. With increasing Co ion ratio from D1 to D3, the dark current and photocurrent both increase, indicating enhanced carrier generation and reduced interfacial barriers, likely due to improved charge transport pathways by enhance fiber connectivity. Notably, sample D3, which contains the highest Co content, exhibits the highest photocurrent response, indicating a significant gain in photoconductivity. The photoconductive gain (G), calculated as the ratio of photocurrent to dark current at the same voltage [34]. The I–V results are consistent with the Hall measurements, confirming that D3 demonstrates superior performance for photoresponse and electrical applications.

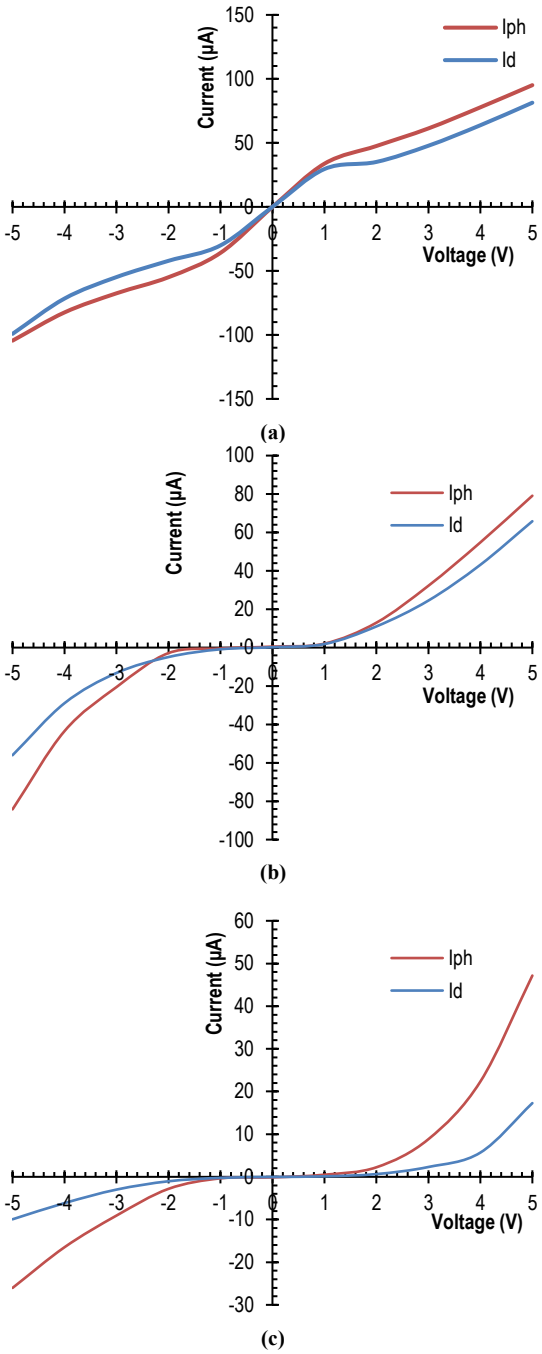

Fig. (5) I-V characteristics of the prepared samples under illumination and in dark conditions of (a) D1, (b) D2, and (c) D3

Table (5) Dark current, light current, and Gain at 5-volt for the Samples D1, D2, and D3

Sample	$I_d \times 10^{-5}$ (A)	$I_{ph} \times 10^{-5}$ (A)	Gain= I_{ph} / I_d
D1	8.139	9.510	1.168
D2	6.581	7.909	1.202
D3	9.942	26.02	2.617

Figure (6) illustrates the current-time (I–t) response of the fabricated photodetectors based on the three

samples under periodic illumination cycles to the UV light. All samples exhibit a distinct and repeatable behavior of nearly square signal. Among them, sample D3 demonstrated the highest photocurrent. The rise time (the time required for the current to increase to 90% of its maximum variation and fall time to 10% of its variations were also evaluated.

Sensitivity (S) is one of the significant parameters that determines the photodetector quality, and is given by [35]:

$$S(\%) = \Delta I_\lambda / I_d \times 100 \quad (4)$$

where $\Delta I_\lambda = I_{light} - I_d$ is the photocurrent, I_{light} is the light current, I_d is the dark current. The sensitivity values of the photodetector were determined according to the current-time response curves, shown in Fig. (6). The sensitivity values were 404%, 211%, and 503.8% for the samples D1, D2, and D3, respectively, with a wavelength of 380 nm at 1 volt. The increased sensitization in D3 could be due to the increased concentration of cobalt ions with the polymer. The photoresponse of the three devices remained consistent over five consecutive light on/off cycles, with negligible current variation (<3%) between cycles, indicating high reproducibility.

Although sample D3 exhibits higher resistivity compared to D2, it demonstrates enhanced photodetector performance, which can be attributed to the reduced energy band gap, which enhances optical absorption and leads to the generation of a greater number of photogenerated charge carriers under illumination. Additionally, the increased cobalt oxide content improves charge transport by enhancing fiber connectivity.

Studies such as that of Pazhanivelu et al. have shown that the concentration of Co^{2+} to ZnO leads to improved structural, optical and magnetic properties. These improvements contribute to the increased optical and magnetic sensitivity of nanofibers [36,37].

The following equations were used to evaluate the performance of the fabricated (Zn,Co):PVA/n-Si sensor photodetector. The quantum efficiency (η) was calculated using the relation [38]:

$$\eta(\lambda) = \frac{1240}{\lambda(\mathrm{nm}) \times R_\lambda} \times 100\% \quad (5)$$

where λ is the wavelength and R_λ is the responsivity

The Noise-Equivalent Power (NEP) equal to:

$$\mathrm{NEP} = \frac{I_n}{R_\lambda} \quad (6)$$

where I_n is the noise current

The Detectivity (D) and Specific Detectivity (D*) were determined using the relations:

$$D = \frac{1}{NEP} \quad (7)$$

$$D^* = \frac{\sqrt{\Delta f . A_d}}{NEP} \quad (8)$$

where A_d is the active area of the detector. Furthermore, incorporating metal oxide nanoparticles into conductive matrices is a key factor in enhancing charge transport. As noted in source [39], this technique significantly improves photodetector performance, leading to better light response and conversion efficiency.

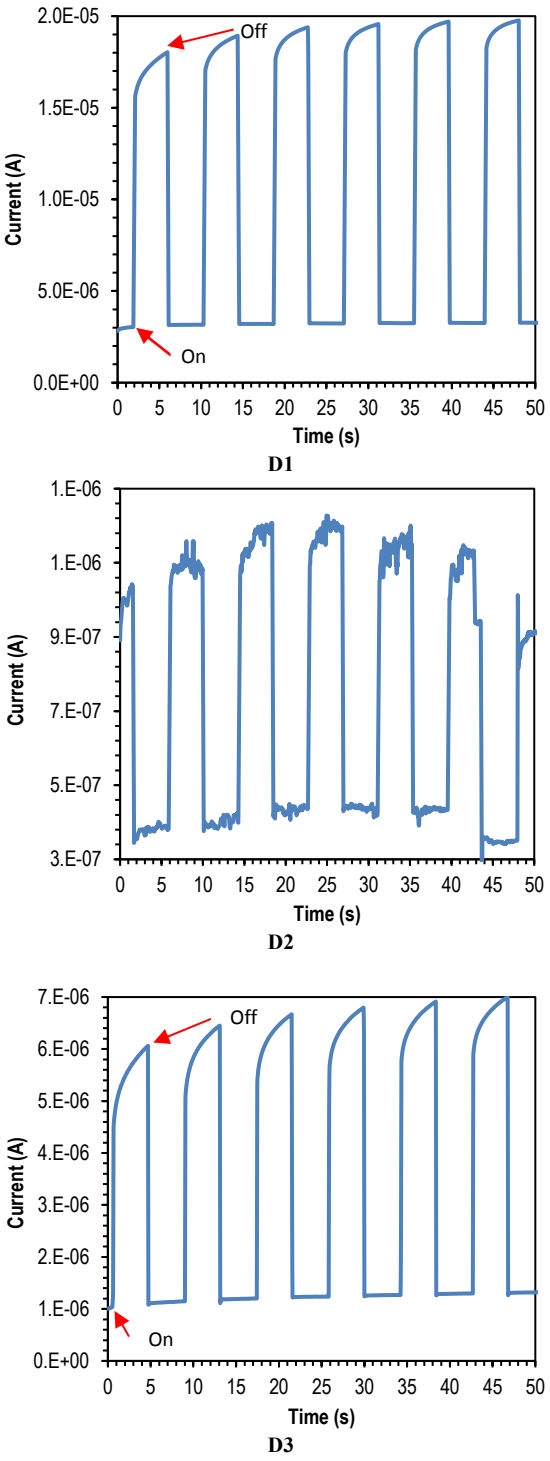

Fig. (6) The current–time curves of the photodetector under on/off switch illumination with wavelengths light 380 nm at 1V bias voltages

Table (6) displays the parameters of the detector based on the samples D1, D2, and D3 at 380 nm wavelengths, including η, NEP, D, D^*. A significant

performance was appeared for the sample D3 compared with the other samples, displaying the highest η value of 16.9%. This is consistent with its highest absorbance and narrowest-energy bandgap. The NEP displays the lowest value 1.05×10^{-11} W of the same sample, indicating improved sensitivity. The detectivity (D) and specific detectivity (D^*) show an increased values for this sample of 9.50×10^{10} (1/W) and 3.98×10^{10} ($cm.Hz^{1/2}.W^{-1}$), respectively.

Table (6) Values of η, NEP, D, and D* for the three samples at 380 nm wavelength

Sample	η (%)	NEP×10^{-11} (W)	D ×10^{10} (1/W)	D*×10^{10} ($cm.Hz^{1/2}.W^{-1}$)
D1	6.2	2.88	3.47	1.45
D2	5.1	3.46	2.89	1.21
D3	16.9	1.05	9.50	3.98

4. Conclusion

(Zn,Co)–PVA nanofibers with varying Co concentrations were successfully synthesized using the electrospinning technique. The formation of uniform nanofibers with diameter variation was revealed depending on dopant concentration. The Co content significantly influenced charge carrier mobility and concentration, with optimal enhancement observed at 20%. The devices exhibit diode-like behavior, achieving the highest photoresponse under visible light, indicating strong photodetection capability for the 40% Co ratio. The tunability of the electrical and optoelectronic properties of the nanofibers was indicated by adjusting the dopant ratio, making them promising candidates for use in flexible photodetectors. The fabricated photodetector, while showing high sensitivity, may face limitations such as long-term stability. Future work will focus on testing environmental durability to enhance device reliability.

References

[1] A. Jailani et al., "Enhancing polyvinyl alcohol (PVA) nanocomposites: Key properties, applications and challenges in advanced engineering", *Def. Technol.,* accepted for publishing (2025), https://doi.org/10.1016/j.dt.2025.05.020.

[2] A. Bin Rashid et al., "Nanotechnology-enhanced fiber-reinforced polymer composites: Recent advancements on processing techniques and applications", *Heliyon,* 10(2) (2024) e24692.

[3] S. Raha and M. Ahmaruzzaman, "ZnO nanostructured materials and their potential applications: progress, challenges and perspectives", *Nanoscale Adv.,* 4(8) (2022) 1868-1925.

[4] Z. Luo et al., "Preparation and Application of Co-Doped Zinc Oxide: A Review", *Molecules,* 29(14) (2024) 3373.

[5] S. Osali, H. Esfahani and H. Karami, "Effect of Al doping on crystallography and electro-optical properties of ZnO semiconductor thin films prepared by electrospinning", *Solid State Sci.,* 83 (2018) 90-98.

[6] V. Pandey et al., "Optical bandgap tuning of cubic spinel Co_3O_4 by annealing temperature", *Materialia,* 26 (2022) 101554.

[7] I.M. Ibrahim, A. Safi and N. Al-Hardan, "Enhancement the sensitivity of CdS nano structure by adding of rare earth materials", *IOP J. Phys. Conf. Ser.,* 1178 (2019) 12013.

[8] Y.O. Naif and I.M. Ibrahim, "Impact of Zn/Sn ion dual incorporation on the functional properties of electrospun PVP nanofibers for photovoltaic sensors", *J. Ovonic Res.,* 21(4) (2025) 387-398.

[9] K.N. Narasimhamurthy et al., "Nanocomposites of PVA-PVP and l-ascorbic acid modified ZnO:Fe via ultrasonic irradiation as a green technique: Latent fingerprint detection, food packing and anti-bacterial applications", *Inorg. Chem. Commun.,* 156 (2023) 111161.

[10] M.D. Thum et al., "Azobenzene-Doped Liquid Crystals in Electrospun Nanofibrous Mats for Photochemical Phase Control", *ACS Appl. Nano Mater.,* 4(1) (2021) 297-304.

[11] Y.O. Naif and I.M. Ibrahim, "Fabrication and characterization of electrospun PVP fibers doped with tin ions for photodetector applications", *J. Opt.*, accepted for publishing (2025), https://doi.org/10.1007/s12596-025-02674-y.

[12] M.S.A. Hamid and I.M. Ibrahim, "Ag-PVP nanofiber for UV Photodetector Produced by Electrospinning Technique", *Iraqi J. Appl. Phys.,* 20(3) (2024) 687–692.

[13] C. Bavatharani et al., "Electrospinning technique for production of polyaniline nanocomposites/nanofibres for multi-functional applications: A review", *Synth. Met.,* 271 (2021) 116609.

[14] S. Santibenchakul, S. Chaiyasith and W. Pecharapa, "PVP-Assisted Sb-Doped SnO_2 Nanofibers Synthesized by Electrospinning Process", *Key Eng. Mater.,* 675-676 (2016) 150-153.

[15] J. Liu et al., "Challenges and recent advances in photodiodes-based organic photodetectors", *Mater. Today,* 51 (2021) 475–503.

[16] Y. Wang and J.J. Santiago-Avilés, "A Review on Synthesis and Characterization of Lead Zirconate Titanate Nanofibers through Electrospinning", *Integr. Ferroelectr.,* 126(1) (2011) 60–76.

[17] M. Teodorescu, M. Bercea and S. Morariu, "Biomaterials of PVA and PVP in medical and pharmaceutical applications: Perspectives and challenges", *Biotechnol. Adv.,* 37(1) (2019) 109-131.

[18] B. Ramdane et al., "Synthesis and characterisation of ZnO/PVA composite nanofibres by

electrospinning", *Int. J. Nanoparticles,* 4 (2011) 10–19.
[19] H. Wang et al., "Preparation and characterization of ZnS:Cu/PVA composite nanofibers via electrospinning", *Mater. Lett.,* 60(20) (2006) 2480–2484.
[20] H.M. Hawy and I.M. Ali, "The role of Ag NPs in PVA electrospun NFs for ultra-high sensitivity photodetector", *Optik*, 262 (2022) 169263.
[21] S.A. Salim et al., "Electrospun zinc-based metal organic framework loaded-PVA/chitosan/hyaluronic acid interfaces in antimicrobial composite nanofibers scaffold for bone regeneration applications", *J. Drug Deliv. Sci. Technol.,* 76 (2022) 103823.
[22] J.-C. Park et al., "Electrospun poly(vinyl alcohol) nanofibers: effects of degree of hydrolysis and enhanced water stability", *Polym. J.,* 42(3) (2010) 273–276.
[23] M. Tahir, S. Vicini and A. Sionkowska, "Electrospun Materials Based on Polymer and Biopolymer Blends - A Review", *Polymers,* 15(7) (2023) 1654.
[24] X. Gong et al., "Characterization of poly(vinyl alcohol) (PVA)/ZnO nanocomposites prepared by a one-pot method", *Compos. B: Eng.,* 60 (2014) 144–149.
[25] G. Nasar, M.S. Khan and U. Khalil, "Structural study of PVA composites with inorganic salts by X-ray diffraction", *J. Pakistan Mater. Soc.,* 3(2) (2009) 67–70.
[26] A.L. Patterson, "The Scherrer Formula for X-Ray Particle Size Determination", *Phys. Rev.,* 56(10) (1939) 978-982.
[27] X. Sui, C. Shao and Y. Liu, "Photoluminescence of polyethylene oxide–ZnO composite electrospun fibers", *Polymer*, 48(6) (2007) 1459–1463.
[28] V. Jacobs, R. Anandjiwala and M. Maaza, "The influence of electrospinning parameters on the structural morphology and diameter of electrospun nanofibers", *J. Appl. Polym. Sci.,* 115 (2010) 3130–3136.
[29] C. Busacca et al., "CO gas sensing performance of electrospun Co_3O_4 nanostructures at low operating temperature", *Sens. Actuat. B: Chem.,* 303 (2020) 127193.
[30] S. Thomas et al., **"Advanced Polymeric Materials: From Macro- to Nano-Length Scales"**, Apple Academic Press (2016).
[31] R.A. Zargar, **"Metal Oxide Nanocomposite Thin Films for Optoelectronic Device Applications"**, Wiley (2023).
[32] V. Kuncser and L. Miu, **"Size Effects in Nanostructures: Basics and Applications"**, Springer (Berlin Heidelberg, 2014).
[33] A.J. Noori and I.M. Ali, "An Investigation on the Rectifying Characteristics of PVA/Y_2O_3 Nanofibers", *Iraqi J. Phys.,* 23(1) (2014) 103–113.
[34] J. Piprek, **"Handbook of Optoelectronic Device Modeling and Simulation: Lasers, Modulators, Photodetectors, Solar Cells, and Numerical Methods"**, vol. 2, CRC Press (2017).
[35] S. Awadalla, **"Solid-State Radiation Detectors: Technology and Applications"**, CRC Press (2017).
[36] V. Pazhanivelu et al., "Influence of Co ions doping in structural, vibrational, optical and magnetic properties of ZnO nanoparticles", *J. Mater. Sci. Mater. Electron.,* 27(8) (2016) 8580–8589.
[37] F.H. Vieii, R.S. Havigh and H.M. Chenari, "Electrospun preparation of nickel and Cobalt-doped ZnO fibers: study on the physical properties", *Sci. Rep.,* 15(1) (2025) 10898.
[38] R.A. Ahmed, N.K. Hassan and I. Ibrahim, "Figure of Merit of UV-Detector for PVP/Nd Nanofiber Prepared by Electrospun Technique", *Des. Eng.,* 1 (2021) 13333–13349.
[39] F.J. Hameed and I.M. Ibrahim, "Synthesis of PPy-MnO_2 Nanocomposite for Utilization in Supercapacitor Applications", *Iraqi J. Phys.*, 22(3) (2024) 67-77.

Table (4) Hall measurement results for the samples D1, D2, and D3

Sample	R_H (m^2/C)	Concentration ($1/cm^3$)	Mobility (cm^2/Vs)	Resistivity ($\Omega.cm$)	Conductivity ($1/\Omega.cm$)	Type
D1	2.90E+07	2.15E+11	1.49E+01	1.95E+05	5.14E-07	P
D2	2.18E+06	2.87E+12	3.53E+01	6.18E+04	1.62E-05	P
D3	-2.60E+07	2.41E+11	1.37E+02	1.90E+05	5.26E-06	N

